Attosecond time delay in atomic photoionization: Angular-dependent transition from dipole to quadrupole and spin-flip dynamics

Rezvan Khademhosseini,[1,*] Pranawa C. Deshmukh,[2,3,†] and Steven T. Manson[1,‡]
[1]*Department of Physics and Astronomy, Georgia State University, Atlanta, Georgia 30303, USA*
[2]*Department of Physics and CAMOST, Indian Institute of Technology Tirupati, Tirupati 517506, India*
[3]*Department of Physics, Dayananda Sagar University, Bengaluru 560114, India*

(Received 18 August 2023; accepted 29 November 2023; published 19 December 2023)

The angular distribution of attosecond Wigner time delay has been investigated including both quadrupole and relativistic effects using the relativistic-random-phase approximation that is based on the Dirac equation and includes significant aspects of many-body correlations. The results show a dramatic evolution of the time delay from (essentially nonrelativistic) dipole to quadrupole and spin-flip dynamics as a function of angle, thereby providing a venue for studying these interactions at the attosecond level.

DOI: 10.1103/PhysRevA.108.063107

I. INTRODUCTION

The interest in attosecond time delay [Wigner-Eisenberg-Smith (WES) time delay [1–3]] in atomic and molecular photoionization was stimulated by experimental measurements which measured time delay at the attosecond level [4,5]. The interest was further enhanced because the study of attosecond time delay provides information on atomic and molecular dynamics on the timescale of the motion of the electrons, and particularly, their behavior while undergoing transitions from one state to another. As a result of these stimuli, there have been a large number of investigations, both experimental and theoretical, of attosecond time delay in atomic and molecular photoionization (see, e.g., [6–27]). This work had been done almost entirely on dipole transitions; in fact, it was reported in one study that "no time delay due to nondipole terms is found" [28]. More recently, nondipole effects in time delay were considered, but only at the nonrelativistic level and for lowest order [25]. In addition, most of the calculations of time delay reported have been performed using nonrelativistic methodologies [26]. However, relativistic and nondipole interactions can be important in time delay, particularly in the angular distribution of the time delay.

An excellent "laboratory" to study this is for *ns* states of closed-shell atoms where the time delay is isotropic, independent of angle, at the nonrelativistic dipole level [25]. In fact, even with the inclusion of relativistic effects at the dipole level, if we look at the dominant transitions, where the spin of the photoelectron in its initial and final states is unchanged (no spin flip), the angular distribution remains isotropic. With the inclusion of spin-flip transitions, engendered by relativistic interactions, along with nondipole effects, the angular distribution is no longer close to isotropic, as shall be seen. Thus, measurements of the angular distribution of time delay for these *ns* states can give detailed information on spin-flip and quadrupole photoionizing transitions, which is normally quite difficult to come by without simultaneously detecting the photoelectron spin and the orientation of the residual ion in coincidence with the time delay. In this article, the photoionization of the 3*s* subshell of Ar is studied to provide a specific example of the phenomenology engendered by the inclusion of spin-flip and quadrupole transitions. This case is of particular interest owing to the Cooper minimum [29] in the cross section which engenders particularly large time delays [7].

II. THEORETICAL DETAILS

The WES photoionization time delay, in atomic units, for a complex transition amplitude $T = |T|e^{i\delta}$ is given by [30]

$$\tau = \frac{d\,\arg[T(E)]}{dE} = \frac{d\delta}{dE}, \tag{1}$$

where E is the photoelectron energy. In the present work the relativistic-random-phase approximation (RRPA) is applied to get the transition matrix elements and the phases of the matrix elements. The RRPA [31–33] takes into account the relativistic effects and also many of the important electron correlations and has been upgraded to deal with both dipole and quadrupole transitions. The RRPA dipole and quadrupole transition matrix elements for $n\kappa \rightarrow E\bar{\kappa}$ transitions are given by

$$\begin{aligned} D_{n\kappa\rightarrow E\bar{\kappa}} &= i^{1-\bar{l}}e^{i\delta_{\bar{\kappa}}} < E,\bar{\kappa}\big|\big|Q_1^{(1)}\big|\big|n\kappa>_{\rm RRPA}, \\ Q_{n\kappa\rightarrow E\bar{\kappa}} &= i^{1-\bar{l}}e^{i\delta_{\bar{\kappa}}} < E,\bar{\kappa}\big|\big|Q_2^{(1)}\big|\big|n\kappa>_{\rm RRPA}, \end{aligned} \tag{2}$$

where $\langle E,\bar{\kappa}||Q_1^{(1)}||n\kappa\rangle_{\rm RRPA}$ and $\langle E,\bar{\kappa}||Q_2^{(1)}||n\kappa\rangle_{\rm RRPA}$ are the reduced matrix element, $\bar{l}$ is the final-state orbital angular momentum, and $\delta_{\bar{\kappa}}$ is the energy-dependent phase of the final-state continuum wave function using incoming wave boundary conditions. The phase $\delta_{\bar{l}}(E)$ of the $\bar{l}$th partial wave,

*rkhademhosseini1@gsu.edu
†pcd@iittp.ac.in
‡smanson@gsu.edu

i.e., the full RRPA dipole matrix element of Eq. (2) is given by

$$\delta_{\bar{l}}(E) = \tan^{-1}\left\{\frac{\mathrm{Im}\langle E,\bar{\kappa}|\hat{d}|n\kappa\rangle}{\mathrm{Re}\langle E,\bar{\kappa}|\hat{d}|n\kappa\rangle}\right\} \tag{3}$$

with a similar expression for quadrupole transitions, $Q_{n\kappa\to E\bar{\kappa}}$, with the proviso that the reduced matrix element operator is then $Q_2^{(1)}$.

The reduced transition amplitudes, $\bar{T}$, for the photoionization of ns states of a closed-shell atom by linearly polarized photons are given for dipole transitions (reduced by omitting common factors which do not affect the time delay removed for simplicity) as

$$\left[\bar{T}_{10}^{1+}\right]_{ns_{1/2}}^{m=1/2} = -\frac{1}{3\sqrt{2}}Y_{10}D_{ns_{1/2}\to\varepsilon p_{1/2}} - \frac{1}{3}Y_{10}D_{ns_{1/2}\to\varepsilon p_{3/2}}, \tag{4a}$$

$$\left[\bar{T}_{10}^{1-}\right]_{ns_{1/2}}^{m=1/2} = \frac{1}{3}Y_{11}D_{ns_{1/2}\to\varepsilon p_{1/2}} - \frac{1}{3\sqrt{2}}Y_{11}D_{ns_{1/2}\to\varepsilon p_{3/2}}, \tag{4b}$$

and for quadrupole transitions as

$$\left[\bar{T}_{20}^{1+}\right]_{ns_{1/2}}^{m=1/2} = -\frac{1}{5}Y_{20}Q_{ns_{1/2}\to\varepsilon d_{3/2}} - \frac{\sqrt{3}}{5\sqrt{2}}Y_{20}Q_{ns_{1/2}\to\varepsilon d_{5/2}}, \tag{5a}$$

$$\left[\bar{T}_{20}^{1-}\right]_{ns_{1/2}}^{m=1/2} = \frac{\sqrt{3}}{5\sqrt{2}}Y_{21}Q_{ns_{1/2}\to\varepsilon d_{3/2}} - \frac{1}{5}Y_{21}Q_{ns_{1/2}\to\varepsilon d_{5/2}}. \tag{5b}$$

The superscripts + and – refer to non-spin-flip (NSF) and spin-flip (SF) transitions, respectively. Note that Eqs. (4) and (5) show the possible final states for dipole and quadrupole transitions implicitly. Combining dipole and quadrupole transitions, the different factors multiplying each must be included, and these are obtained from Eq. (43) of [31], and the total no-spin-flip and spin-flip amplitudes are given by

$$[\bar{T}^{+}]_{ns_{1/2}}^{m=1/2} = \frac{\sqrt{2}}{\sqrt{3}}\left[\bar{T}_{10}^{1+}\right]_{ns_{1/2}}^{m=1/2} + \frac{\alpha h\nu}{\sqrt{30}}\left[\bar{T}_{20}^{1+}\right]_{ns_{1/2}}^{m=1/2} = \bar{T}^{+}, \tag{6a}$$

$$[\bar{T}^{-}]_{ns_{1/2}}^{m=1/2} = \frac{\sqrt{2}}{\sqrt{3}}\left[\bar{T}_{10}^{1-}\right]_{ns_{1/2}}^{m=1/2} + \frac{\alpha h\nu}{\sqrt{30}}\left[\bar{T}_{20}^{1}\right]_{ns_{1/2}}^{m=1/2} = \bar{T}^{-}, \tag{6b}$$

where α is the fine-structure constant, $\sim 1/137$, and $h\nu$ is the photon energy in atomic units (27.21 eV). The time delays can then be calculated via Eq. (1) yielding angle-dependent $\tau^{+}(\theta)$ and $\tau^{-}(\theta)$,

$$\text{NSF time delay } \tau^{+} = \frac{d}{dE}\arg\left[\bar{T}^{+}\right]_{ns_{1/2}}^{m=1/2}, \tag{7a}$$

$$\text{SF time delay } \tau^{-} = \frac{d}{dE}\arg\left[\bar{T}^{-}\right]_{ns_{1/2}}^{m=1/2} \tag{7b}$$

$$\text{NSF dipole time delay } \tau_{\mathrm{dip}}^{+} = \frac{d}{dE}\arg\left[\bar{T}_{10}^{1+}\right]_{ns_{1/2}}^{m=1/2}, \tag{7c}$$

θ being the angle between the photoelectron direction and the photon polarization. Note that the time delay can, in principle, be measured individually in a coincidence experiment, coincident with both the orientation of the residual ion and the spin direction of the photoelectron. For the case where coincidence is not done, the total time delay, averaged over both no-spin-flip τ^{+} and spin-flip τ^{-} channels is given by [29]

$$\tau(\theta) = \frac{|[\bar{T}^{+}]_{ns_{1/2}}^{m=1/2}|^2\tau^{+} + |[\bar{T}^{-}]_{ns_{1/2}}^{m=1/2}|^2\tau^{-}}{|[\bar{T}^{+}]_{ns_{1/2}}^{m=1/2}|^2 + |[\bar{T}^{-}]_{ns_{1/2}}^{m=1/2}|^2}. \tag{8}$$

Note that the usually dominant transition amplitude in the photoionization, $[T_{10}^{1+}]_{ns_{1/2}}^{m=1/2}$, depends upon Y_{10}, which vanishes at $\theta = 90^{\circ}$. Thus, at this angle, perpendicular to the photon polarization, τ^{+} is determined entirely by quadrupole transitions, and the total time delay, thus, depends on quadrupole and spin-flip transitions.

III. RESULTS AND DISCUSSION

The Ar $3s$ calculations were performed using RRPA as mentioned. All single excitation/ionization channels were included and coupled, i.e., interchannel coupling in the final state. Specifically,

$$np_{1/2}\to\varepsilon s_{1/2},\varepsilon d_{3/2};\quad np_{3/2}\to\varepsilon s_{1/2},\varepsilon d_{3/2},\varepsilon d_{5/2};$$
$$n=2,3,ns_{1/2}\to\varepsilon p_{1/2},\varepsilon p_{3/2};\quad n=1{-}3$$

for the 16 dipole channels and

$$np_{1/2}\to\varepsilon p_{3/2},\varepsilon f_{3/2};\quad np_{3/2}\to\varepsilon p_{1/2},\varepsilon p_{3/2},\varepsilon f_{5/2},\varepsilon f_{7/2};$$
$$n=2,3,ns_{1/2}\to\varepsilon d_{3/2},\varepsilon d_{5/2};\quad n=1{-}3$$

for the 18 quadrupole channels. As a practical matter, at the low energies that are considered here, the $1s$ channels are essentially irrelevant in both dipole and quadrupole cases.

For reference, the Ar $3s$ photoionization cross section exhibits a Cooper minimum at a photon energy of about 41 eV [34,35]. Furthermore, it is useful to point out that the RRPA calculation gives excellent agreement with this cross section generally and, in particular, in the neighborhood of the Cooper minimum [36]. As for the photoelectron angular distribution asymmetry parameter, β, the available experimental data [37] exhibits large error bars and is consistent with $\beta = 2$ over a broad energy range which coincides with the RRPA results [36]. In other words, The RRPA calculation agrees with experiment for both the Ar $3s$ cross section and the β parameter, which suggests that the RRPA matrix elements should be accurate in the calculation of time delay as well.

The results of our calculations for WES time delay at 38 eV, close to but below the Cooper minimum, are displayed in Fig. 1 at four levels of approximation. The lowest level, no-spin-flip dipole, τ_{dip}^{+}, Eq. (7c), is seen to be angle independent at a value of about 260 as (attoseconds); this is substantially the same as the nonrelativistic dipole result [11]. The total no-spin-flip time delay, τ^{+}, which includes quadrupole effects, Eq. (7a), paints a vastly different picture being very strongly a function of angle and traversing time delays from close to -190 as to about 350 as, a change in time delay of more than 500 as over a rather small angular range. The largest deviations are in the region of 90°, perpendicular to the photon polarization, where the dipole contribution to τ^{+} vanishes. But it is noteworthy that the quadrupole contribution is still in evidence at 0°. The fact that the quadrupole contribution vanishes at the "magic angles" ($\sim 57^{\circ}$ and 123° degrees), is the reason that τ^{+} and the no-spin-flip dipole time delay, τ_{dip}^{+}, are equal at those angles, i.e., this is purely an effect of

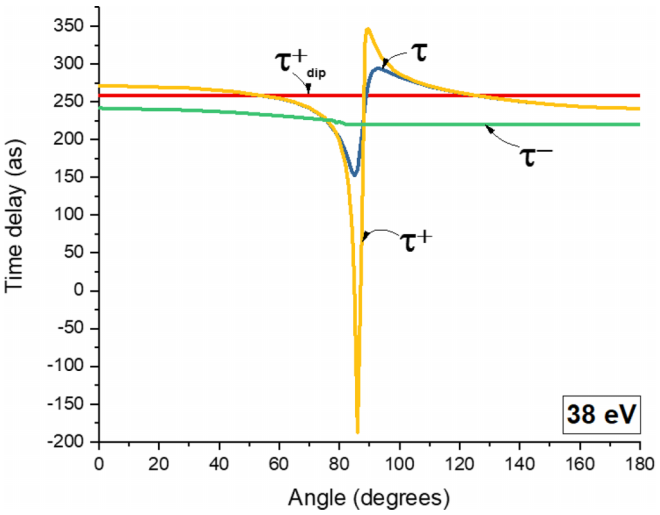

FIG. 1. Calculated time delay for Ar 3*s* at 38 eV photon energy for linearly polarized photons as a function of angle with respect to photon polarization showing the total time delay, τ, the no-spin-flip time delay, τ^+, the spin-flip time delay, τ^-, and the no-spin-flip dipole time delay, $\tau^+_{\rm dip}$.

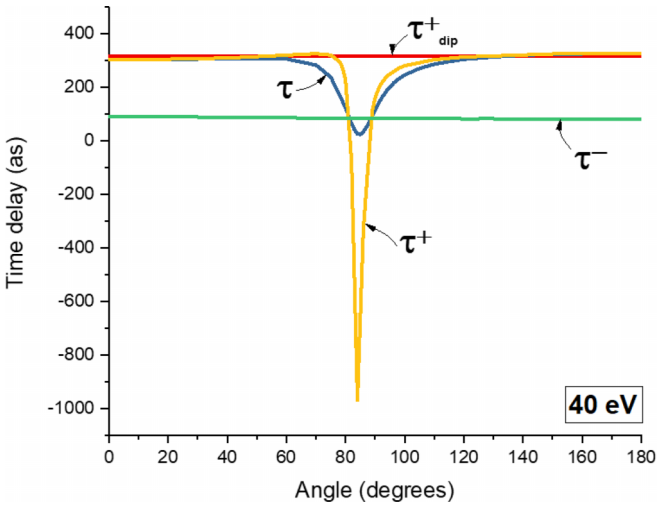

FIG. 2. As Fig. 1 except for a photon energy of 40 eV.

(angular momentum) geometry. Looking at the total spin-flip time delay, τ^-, coming from Eq. (7b), only a weak angular dependence is seen. Note also, it is seen from the above equations, that without the quadrupole contribution, τ^- would be independent of angle as well, so the weak angular dependence is a result of quadrupole interactions.

The total time delay, $\tau(\theta)$, shown in Fig. 1 and given by Eq. (8), is seen to be essentially identical to τ^+ except in the angular range from 80° to 100°. This occurs because outside this range, the magnitude of $\bar{T}^+$ is much larger than $\bar{T}^-$ since the former is dominated by the dipole no-spin-flip transitions. However, owing to angular momentum geometry, the dipole no-spin-flip amplitude, $[\bar{T}^{1+}_{10}]^{m=1/2}_{ns_{1/2}}$, vanishes at 90°, and the relative contribution of $\bar{T}^-$ becomes much more important in this angular range. And, since $\tau(\theta)$ is a linear combination of τ^+ and τ^-, Eq. (8), its value must lie between them, which is clearly seen in Fig. 1. It is also evident that in the angular range around 90°, the quadrupole no-spin-flip and the dipole spin-flip amplitudes are of comparable magnitude; the fact that the spin-flip time delay, τ^-, is relatively flat as a function of angle near 90° translates to a total time delay, $\tau(\theta)$, that varies over a rather smaller but still significant time delay range, about 150–300 as, or a roughly 150 as traverse, as compared to τ^+. However, the shape of the angular distribution of the total time delay $\tau(\theta)$ is similar to the shape of the no-spin-flip time delay τ^+ but significantly truncated. In any case, it is quite clear that the inclusion of relativistic spin-flip and quadrupole effects dramatically alters the angular dependence of the WES time delay.

As a next example, the situation for a photon energy of 40 eV, a scant 2 eV above the situation discussed above, is shown in Fig. 2 where it is evident that the effects of spin-flip and quadrupole transitions are quite important, although the detailed shapes are rather different than the preceding case. At 40 eV, being closer to the Cooper minimum, the dynamics are somewhat different. Of course, owing to (angular momentum) geometry, $\tau^+_{\rm dip}$ is isotropic, and it is rather large as time delays go—more than 300 as. In addition, τ^+ exhibits a huge traverse, in the 90° region, going from ∼300 as to almost −1000 as (and back) over a small angular range, owing to the quadrupole transitions. Furthermore, the shape is completely different, reflecting the different dynamics between the two energies. The spin-flip time delay, τ^-, is essentially isotropic because the quadrupole contribution is significantly smaller than the dipole, at this energy, somewhat different than at 38 eV where a weak angular dependence of τ^- is seen. The total time delay is again similar in shape to τ^+ although much truncated, but still, a very large variation of ∼300 as in the 90° region. Thus, it is seen that the details of the angular dependence of the time delay is extremely sensitive to dynamics.

Moving away from the Cooper minimum region, the time delay for photon energies of 90.07 and 120 eV are presented in Fig. 3 where it is seen that the whole scale of the time delay is reduced rather considerably. In addition, only a restricted range of angles is shown since, at these energies, the spin-flip and quadrupole channels only engender significant angular dependence in the 90° region. The value of $\tau^+_{\rm dip}$ hardly changes from one energy to the other, but the detailed dynamics are very different. This is reflected in the rather asymmetric shape of τ^+ and, thus, τ as functions of angle for the lower energy, but a symmetric shape for the higher energy.

To get a better feel for the evolution of the total time delay, τ, with energy and angle, Fig. 4 depicts the situation for a variety of energies from 38 to 269.9 eV, where it is seen that the shapes and magnitudes of the time delay vary substantially with energy as a result of the differing dynamics for the various energies. The overall magnitudes of the time delays diminish markedly with energy above the Cooper minimum region, and the angular distributions also change significantly. In the Cooper minimum region, a strong angular dependence of the time delay is seen in Fig. 4 over the entire angular region, from 0 to 180°. This occurs owing to the dynamics in the region of the Cooper minimum, $[\bar{T}^{1+}_{10}]^{m=1/2}_{ns_{1/2}}$, is quite small so that the quadrupole and spin-flip contributions are proportionally larger, and they affect the angular distribution

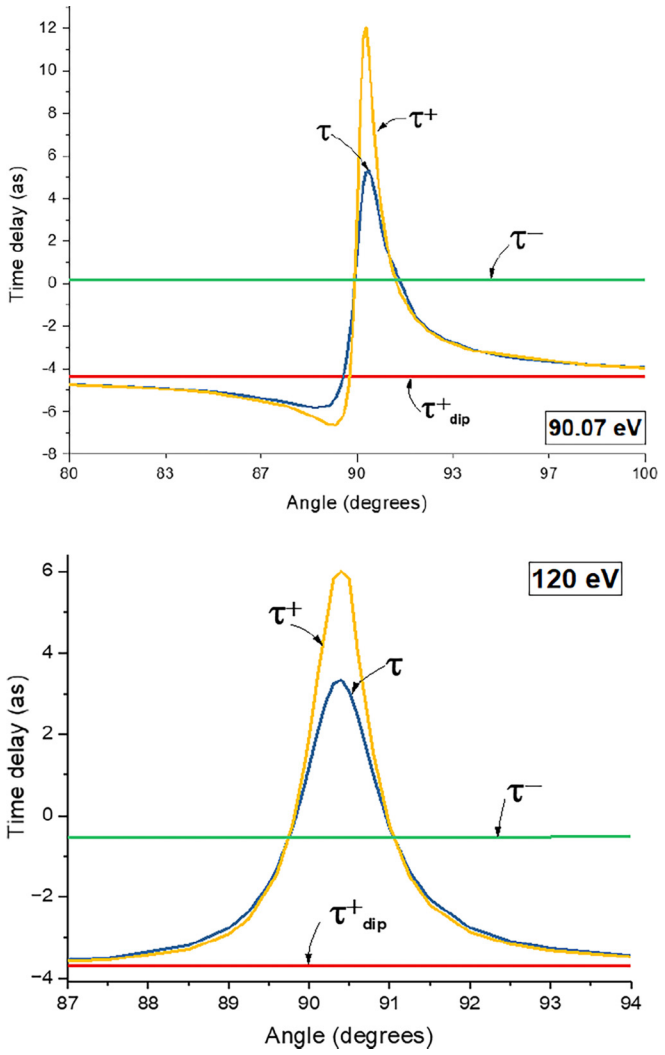

FIG. 3. As Fig. 1 except for photon energy 90.07 eV (upper plot) and 120 eV (lower plot). Note the restrictive range of angles as opposed to the previous plots.

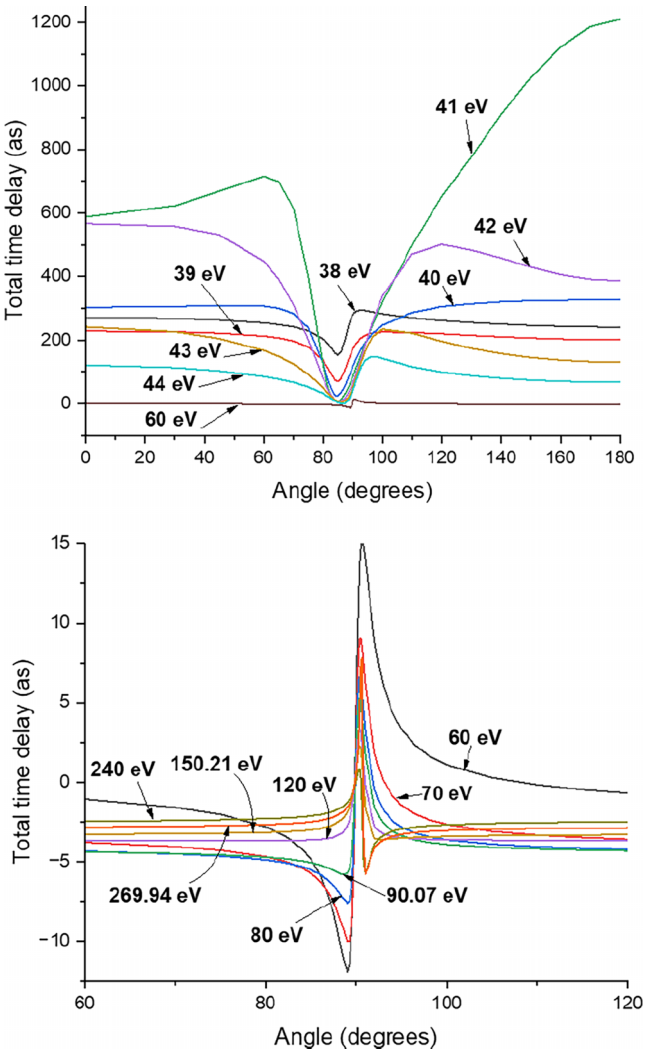

FIG. 4. Total time delay, τ, for a variety of energies as functions of the angle. Note the differing vertical scales on the upper and lower plots.

over the broad range, as seen. With increasing energy, this is no longer the case, so then it is only close to 90°, where $[\bar{T}_{10}^{1+}]_{ns_{1/2}}^{m=1/2}$ vanishes owing to (angular momentum) geometry, where the quadrupole and spin-flip transitions are important. Outside this angular region, the time delay is essentially equal to $\tau_{\rm dip}^{+}$ and the angular distribution is seen to be flat.

It should be mentioned that spin-flip transitions in the context of WES time delay in atomic photoionization have been studied previously in connection with Xe 4*d* photoemission [38]. It was shown there that the spin-flip channels behaved very differently from the no-spin-flip channels. Likewise, in a theoretical investigation in the vicinity of the second Cooper minimum in the Xe 5*s* cross section [39], the spin-flip channel was found to differ considerably from the no-spin-flip channel. In neither of these studies was the angular distribution looked at, however.

It is also important to consider the limitations of the present calculation *vis-à-vis* experiment. At the current level of experimental technology, time delay is investigated by various techniques using two photons: an XUV photon to ionize the system plus an IR photon [14]. And it has been shown recently that this second photon can contribute to or alter the angular distribution of time delay [40]. Thus, while in the nonrelativistic approximation, the single-photon ionization of an *ns* state from a closed-shell atom is isotropic, the two-photon angular distribution is not [40]. In addition, there are other two-photon effects, like a nonlinear (two-photon) Cooper minimum, that have been predicted [41]. Thus, it might require a more complicated experiment, possibly a coincidence experiment, to distinguish between the two-photon effects and the spin-flip and quadrupole effects discussed here.

IV. CONCLUDING REMARKS

In summary then, a fully relativistic study of the angular distribution of WES time delay arising from the photoionization of *ns* states of closed-shell atoms by linearly polarized electromagnetic radiation reveals a complex pattern owing to dynamics and angular momentum geometry. In the region of

90°, perpendicular to the photon polarization, the total time delay, averaged over no-spin-flip and spin-flip transitions, is controlled mostly or completely by quadrupole and spin-flip transitions. Using the example of Ar 3*s*, these effects were seen to be strongest in the energy region of the Cooper minimum. Furthermore, much larger effects were seen in the no-spin-flip time delay, but this will be difficult to investigate experimentally since it would require a coincidence experiment. It is worthwhile to reiterate that at the nonrelativistic dipole level, the WES time delay is isotropic; thus, any variations with angle are indicative of relativistic and/or quadrupole interactions. The importance of relativistic effects is accentuated in the context of either greater speeds or greater atomic number. The present study reveals its importance in the context of geometry. In any case, the study of angular distribution of time delay in the 90° region reveals information on spin-flip and quadrupole transitions at the attosecond level, the natural timescale of the motion of atomic and molecular electrons. And these results are quite general and will apply to *ns* subshells of any closed-shell atom. Finally, we note that studies of other cases are in progress. In addition, we are looking at what additional information might be obtained by the use of circularly polarized light. Furthermore, we are investigating what effects quadrupole transitions might have on *np*, *nd*, and *nf* time delays.

ACKNOWLEDGMENT

This work was supported by the U.S. Department of Energy, Office of Basic Sciences, Division of Chemical Science, Geosciences and Biosciences under Grant No. DE-FG02-03ER15428.

[1] L. Eisenbud, The formal properties of nuclear collisions, dissertation (Princeton University, 1948) (unpublished).
[2] E. P. Wigner, Lower limit for the energy derivative of the scattering phase shift, Phys. Rev. **98**, 145 (1955).
[3] F. T. Smith, Lifetime matrix in collision theory, Phys. Rev. **118**, 349 (1960).
[4] M. Schultze, M. Fieß, N. Karpowicz, J. Gagnon, M. Korbman, M. Hofstetter, S. Neppl, A. L. Cavalieri, Y. Komninos, Th. Mercouris, C. A. Nicolaides, R. Pazourek, S. Nagele, J. Feist, J. Burgdörfer, A. M. Azzeer, R. Ernstorfer, R. Kienberger, U. Kleineberg, E. Goulielmakis, F. Krausz, and V. S. Yakovlev, Delay in photoemission, Science **328**, 1658 (2010).
[5] K. Klunder, J. M. Dahlström, M. Gisselbrecht, T. Fordell, M. Swoboda, D. Guénot, P. Johnsson, J. Caillat, J. Mauritsson, A. Maquet, R. Taïeb, and A. L'Huillier, Probing single-photon ionization on the attosecond time scale, Phys. Rev. Lett. **106**, 143002 (2011).
[6] L. R. Moore, M. A. Lysaght, J. S. Parker, H. W. van der Hart, and K. T. Taylor, Time delay between photoemission from the 2*p* and 2*s* subshells of neon, Phys. Rev. A **84**, 061404(R) (2011).
[7] D. Guénot, K. Klunder, C. L. Arnold, D. Kroon, J. M. Dahlström, M. Miranda, T. Fordell, M. Gisselbrecht, P. Johnsson, J. Mauritsson, E. Lindroth, A. Maquet, R. Taïeb, A. L'Huillier, and A. S. Kheifets, Photoemission-time-delay measurements and calculations close to the 3*s*-ionization-cross-section minimum in Ar, Phys. Rev. A **85**, 053424 (2012).
[8] T. Carette, J. M. Dahlström, L. Argenti, and E. Lindroth, Multiconfigurational Hartree-Fock close-coupling ansatz: Application to the argon photoionization cross section and delays, Phys. Rev. A **87**, 023420 (2013).
[9] A. S. Kheifets, Time delay in valence-shell photoionization of noble-gas atoms, Phys. Rev. A **87**, 063404 (2013).
[10] P. C. Deshmukh, A. Mandal, S. Saha, A. S. Kheifets, V. K. Dolmatov, and S T Manson, Attosecond time delay in the photoionization of endohedral atoms A@C_{60}: A new probe of confinement resonances, Phys. Rev. A **89**, 053424 (2014).
[11] S. Saha, A. Mandal, J. Jose, H. R. Varma, P. C. Deshmukh, A. S. Kheifets, V. K. Dolmatov, and S. T. Manson, Relativistic effects in photoionization time delay near the Cooper minimum of noble-gas atoms, Phys. Rev. A **90**, 053406 (2014).
[12] D. Guénot, D. Kroon, E. Balogh, E. W. Larsen, M. Kotur, M. Miranda, T. Fordell, P. Johnsson, J. Mauritsson, M. Gisselbrecht, K. Varjù, C. L. Arnold, T. Carette, A. S. Kheifets, E. Lindroth, A. L'Huillier, and J. M. Dahlström, Measurements of relative photoemission time delays in noble gas atoms, J. Phys. B **47**, 245602 (2014).
[13] T. Barillot, C. Cauchy, P.-A. Hervieux, M. Gisselbrecht, S. E. Canton, P. Johnsson, J. Laksman, E. P. Mansson, J. M. Dahlström, M. Magrakvelidze, G. Dixit, M. E. Madjet, H. S. Chakraborty, E. Suraud, P. M. Dinh, P. Wopperer, K. Hansen, V. Loriot, C. Bordas, S. Sorensen, and F. Lépine, Angular asymmetry and attosecond time delay from the giant plasmon resonance in C_{60} photoionization, Phys. Rev. A **91**, 033413 (2015).
[14] R. Pazourek, S. Nagele, and J. Burgdörfer, Attosecond chronoscopy of photoemission, Rev. Mod. Phys. **87**, 765 (2015), and references therein.
[15] A. S. Kheifets, S. Saha, P. C. Deshmukh, D. A. Keating, and S. T. Manson, Dipole phase and photoelectron group delay in inner shell photoionization, Phys. Rev. A **92**, 063422 (2015).
[16] M. Magrakvelidze, Md. E.-A. Madjet, and H. S. Chakraborty, Attosecond delay of xenon 4*d* photoionization at the giant resonance and Cooper minimum, Phys. Rev. A **94**, 013429 (2016).
[17] M. Ossiander, F. Siegrist, V. Shirvanyan, R. Pazourek, A. Sommer, T. Latka, A. Guggenmos, S. Nagele, J. Feist, J. Burgdörfer, R. Kienberger, and M. Schultze, Attosecond correlation dynamics, Nat. Phys. **13**, 280 (2017).
[18] M. F. Ciappina, J. A. Pérez-Hernández, A. S. Landsman, W. A. Okell, S. Zherebtsov, B. Förg, J. Schötz, L. Seiffert, T. Fennel, T. Shaaran, T. Zimmermann, A. Chacón, R. Guichard, A. Zaïr, J. W. G. Tisch, J. P. Marangos, T. Witting, A. Braun, S. A. Maier, L. Roso, M. Krüger, P. Hommelhoff, M. F. Kling, F. Krausz, and M. Lewenstein, Attosecond physics at the nanoscale, Rep. Prog. Phys. **80**, 054401 (2017), and references therein.
[19] D. A. Keating, P. C. Deshmukh, and S. T. Manson, Wigner time delay and spin-orbit-activated confinement resonances, J. Phys. B **50**, 175001 (2017).
[20] E. Lindroth and J. M. Dahlström, Attosecond delays in laser-assisted photodetachment from closed-shell negative ions, Phys. Rev. A **96**, 013420 (2017).

[21] M. Isinger, R. J. Squibb, D. Busto, S. Zhong, A. Harth, D. Kroon, S. Nandi, C. L. Arnold, M. Miranda, J. M. Dahlström, E. Lindroth, R. Feifel, M. Gisselbrecht, and A. L'Huillier, Photoionization in the time and frequency domain, Science **358**, 893 (2017), and references therein.

[22] D. M. Villeneuve, Attosecond science, Contemp. Phys. **59**, 47 (2018), and references therein.

[23] D. A. Keating, S. T. Manson, V. K. Dolmatov, A. Mandal, P. C. Deshmukh, F. Naseem, and A. S. Kheifets, Intershell-correlation-induced time delay in atomic photoionization, Phys. Rev. A **98**, 013420 (2018).

[24] M. Fanciulli and J. Hugo Dil, Determination of the time scale of photoemission from the measurement of spin polarization, SciPost Phys. **5**, 58 (2018).

[25] A. Kheifets, Time-resolved theory of atomic and molecular photoionization for RABBITT and Attoclock, in *Quantum Collisions and Confinement of Atomic and Molecular Species, and Photons*, Springer Proceedings in Physics, edited by P. Deshmukh, E. Krishnakumar, S. Fritzsche, M. Krishnamurthy, and S. Majumder (Springer, Singapore, 2019), Vol. 230, pp. 1–19, and references therein; M. Ya. Amusia and L. V. Chernysheva, Nondipole effects in time delay of photoelectrons from atoms, negative ions, and endohedrals, JETP Lett. **112**, 673 (2020).

[26] P. C. Deshmukh, S. Banerjee, A. Mandal, and S. T. Manson, Wigner-Eisenbud-Smith time delay in atom-laser interactions, Eur. Phys. J.: Spec. Top. **230**, 4151 (2021), and references therein.

[27] F. Holzmeier, J. Joseph, J. C. Houver, M. Lebech, D. Dowek, and R. R. Lucchese, Influence of shape resonances on the angular dependence of molecular photoionization delays, Nat. Commun. **12**, 7343 (2021).

[28] M. D. Spiewanowski and L. B. Madsen, Nondipole effects in attosecond photoelectron streaking, Phys. Rev. A **86**, 045401 (2012).

[29] J. W. Cooper, Photoionization from outer atomic subshells. A model study, Phys. Rev. **128**, 681 (1962).

[30] A. Kheifets, A. Mandal, P. C. Deshmukh, V. K. Dolmatov, D. A. Keating, and S. T. Manson, Relativistic calculations of angular dependent photoemission time delay, Phys. Rev. A **94**, 013423 (2016).

[31] W. R. Johnson and C. D. Lin, Multichannel relativistic random-phase approximation for the photoionization of atoms, Phys. Rev. A **20**, 964 (1979).

[32] W. R. Johnson and K. T. Cheng, Relativistic effects on low-energy $5s \rightarrow \varepsilon p$ photoionization for xenon, Phys. Rev. Lett. **40**, 1167 (1978).

[33] W. R. Johnson, C. D. Lin, K. T. Cheng, and C. M. Lee, Relativistic random-phase approximation, Phys. Scr. **21**, 409 (1980).

[34] A. Fahlman, T. A. Carlson, and M. O. Krause, Angular distribution of Xe $5s \rightarrow \varepsilon p$ photoelectrons: Disagreement between experiment and theory, Phys. Rev. Lett. **50**, 1114 (1983).

[35] T. Gustafsson, Photoionization cross sections of the $5s$ electrons in Xe measured with synchrotron radiation, Chem. Phys. Lett. **51**, 383 (1977).

[36] W. R. Johnson and K. T. Cheng, Photoionization of the outer shells of neon, argon, krypton, and xenon using the relativistic random-phase approximation, Phys. Rev. A **20**, 978 (1979).

[37] B. Möbus, B. Magel, K.-H. Schartner, B. Langer, U. Becker, M. Wildberger, and H. Schmoranzer, Measurements of absolute Ar $3s$ photoionization cross sections, Phys. Rev. A **47**, 3888 (1993).

[38] S. Zhong, J. Vinbladh, D. Busto, R. J. Squibb, M. Isinger, L. Neoričić, H. Laurell, R. Weissenbilde, C. L. Arnold, R. Feifel, J. M. Dahlström, G. Wendin, M. Gisselbrecht, E. Lindroth, and A. L'Huillier, Attosecond electron–spin dynamics in Xe $4d$ photoionization, Nat. Commun. **11**, 5042 (2020).

[39] A. Ganesan, S. Banerjee, P. C. Deshmukh, and S. T. Manson, Photoionization of Xe $5s$: Angular distribution and Wigner time delay in the vicinity of the second Cooper minimum, J. Phys. B **53**, 225206 (2020).

[40] S. Heuser, À. Jiménez Galán, C. Cirelli, C. Marante, M. Sabbar, R. Boge, M. Lucchini, L. Gallmann, I. Ivanov, A. S. Kheifets, J. M. Dahlström, E. Lindroth, L. Argenti, F. Martín, and U. Keller, Angular dependence of photoemission time delay in helium, Phys. Rev. A **94**, 063409 (2016).

[41] J. Hofrucker, A. V. Volotka, and S. Fritzsche, Breakdown of the electric dipole approximation at Cooper minima in direct two-photon ionization, Sci. Rep. **10**, 3617 (2020).